Weakly-Textured Cylindrical Object Reconstruction via Multi-View Tangent Dihedral Angle Constraints

Xinbo Zhao¹, Lei Qin¹, Yansong Duan^{1,2,*}

¹School of Remote Sensing and Information Engineering, Wuhan University, Wuhan 430079, China - simple_zhao@whu.edu.cn, qinlei@whu.edu.cn, ysduan@whu.edu.cn

²Hubei Luojia Laboratory, Wuhan China

Keywords: Cylindrical Object, Weakly-textured Surface, Dihedral Angle, 3D Reconstruction.

Abstract

Artificial cylindrical structures such as bridge cables and traffic poles constitute critical targets in surveying and emergency response applications, necessitating accurate 3D reconstruction. Current laser scanning solutions face limitations in cost-effectiveness and operational precision, hindering widespread adoption. UAV photogrammetry, leveraging multi-view imagery, shows promise for cylindrical reconstruction but struggles with texture-deficient surfaces and slender geometries, often resulting in distorted models due to insufficient feature matching. This paper introduces a novel framework that exploits bilateral edge features and camera optical centers to construct tangent dihedral angles (TDAs) for cylindrical objects. By establishing correspondence of homologous TDAs across multi-view images, cylindrical geometric parameters are solved under multi-perspective tangency constraints, followed by polygonal mesh generation. The proposed method eliminates dependence on surface textures, achieving millimeter-level diameter estimation accuracy and superior modeling fidelity compared to conventional Multi-View Stereo (MVS) approaches. Experimental validation on bridge cables demonstrates robust reconstruction of slender cylindrical structures under challenging imaging conditions, offering practical value for infrastructure digitization and safety monitoring.

1. Introduction

High-accuracy 3D models serve as fundamental data for virtual reality (VR) technology and digital twins. With technological advancements, the granularity of 3D reconstruction in surveying and mapping has progressively evolved from terrain-level and city-level modeling to component-level and object-level (Ham et al., 2019). Artificial cylindrical structures such as stay cables (Hu et al., 2021), traffic poles (Harshit et al., 2021), and power lines (Inoue et al., 2021) - representative examples of human-made cylindrical objects (Liang et al., 2012; Polat and Uysal, 2020; Sarı et al., 2020) – constitute critical object-level elements in realworld scenarios (Miglani et al., 2013; Polat and Uysal, 2020; Yan et al., 2010). These structures not only represent essential scene details (Berveglieri and Tommaselli, 2018; Nurunnabi et al., 2017) but also serve as crucial monitoring objects for safety management, holding significant importance reconstruction tasks (Langhammer et al., 2018).

However, accurate 3D reconstruction of cylindrical objects currently faces significant challenge. The two primary technologies for object-level 3D reconstruction are laser scanning and UAV photogrammetry. Terrestrial Laser Scanning (TLS) (Rabbani et al., 2006; Rabbani and Van Den Heuvel, 2005; Yan et al., 2010) remains one of the few effective methods for acquiring detailed 3D information of cylindrical objects. Nevertheless, TLS sampling density and positioning accuracy exhibit inverse proportionality with scanning distance, making it difficult to ensure reconstruction completeness and accuracy for distant objects (Nurunnabi et al., 2017). While UAV-borne laser scanning alleviates distance limitations inherent in TLS, the absolute positioning accuracy of UAV-acquired point clouds is fundamentally constrained by platform positioning accuracy, typically limited to 2 cm - insufficient for capturing highaccuracy cylindrical surfaces (Derpanis, 2010). Furthermore, laser scanning cannot capture surface texture and incurs substantially higher operational costs compared to UAV photogrammetry, making the latter more prevalent for detailed object reconstruction.

UAV photogrammetry utilizes high-resolution multi-view imagery (Sarı et al., 2020) as input, theoretically achieving positioning accuracy comparable to image sampling resolution. This technique demonstrates potential for cylindrical structure reconstruction (Castillo et al., 2013; Kattenborn et al., 2014). Although existing UAV-based 3D reconstruction methods have achieved excellent modeling results in most scenarios (Furukawa et al., 2010; Furukawa and Hernández, 2015; Jiang et al., 2022), artificial cylindrical objects present unique challenges. Their typically weakly-textured surfaces and slender geometries (Miglani et al., 2013) lead to insufficient reliable feature points in conventional Multi-View Stereo (MVS) reconstruction, resulting in distorted geometry and texture artifacts (Langhammer et al., 2018), ultimately failing to accurately reproduce cylindrical details (Berra and Peppa, 2020). These reconstruction deficiencies often necessitate manual editing and refinement, significantly increasing economic costs.

Addressing the challenges in 3D modeling of weakly-textured cylindrical structures within complex scenes, and considering the limitations of dense feature-matching-based MVS methods, this paper proposes a novel cylindrical object 3D reconstruction method based on tangent dihedral angle (TDA) constraints, which utilizes edges instead of points as the input feature.

Specifically, the method involves:

- Performing sparse reconstruction of UAV images using existing software to recover camera intrinsics and poses.
- Extracting and pairing edge features in the images.
- Constructing tangent dihedral angles for cylindrical objects using paired edge features from both sides of a cylinder and the corresponding camera optical center.
- Establishing correspondence of tangent dihedral angles across multiple views using sparse reconstruction parameters.
- Solving cylinders' parameters under tangent geometric constraints provided by multi-view TDAs.
- Reconstructing cylinders' mesh models based on images and solved parameters.

The key stages of each process of the proposed method is illustrated in Figure 1.

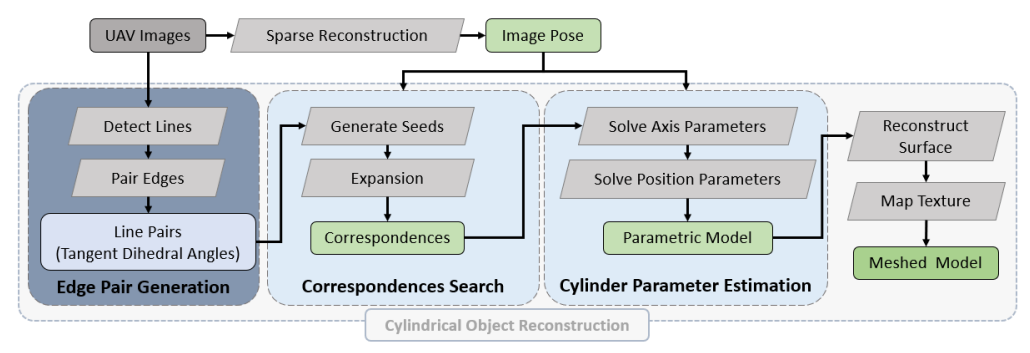


Figure 1. Overview of the proposed method.

2. Related Work

3D reconstruction from UAV imagery constitutes a vital technique in 3D modeling, with its workflow encompassing four stages: feature extraction, sparse reconstruction, dense reconstruction, and meshing. While sparse reconstruction have reached relative maturity and existing dense reconstruction methods achieve satisfactory results in large-scale scenes, the reconstruction quality of tiny targets (e.g., slender cylindrical objects) remains constrained by resolution limitations and texture deficiency. As fundamental geometric primitives in complex structures (Ladrón de Guevara et al., 2011), cylindrical objects present reconstruction challenges for classical approaches, necessitating specialized modeling algorithms (Chuang et al., 2004). Current methodologies can be categorized into two paradigms: dense point cloud-based reconstruction and sparse feature-based reconstruction.

Dense point cloud-based cylindrical reconstruction methods typically assume cylindrical surface points follow a normal distribution and employs least-squares cylinder fitting (Marshall et al., 2001), followed by mesh generation from optimized parameters. This approach has been applied to achieve fully automatic cylindrical tree trunk reconstruction, though suboptimal accuracy persists due to point cloud quality limitations (Liang et al., 2012). Adaptive least-squares matching has also been utilized to model the conic-section-like variations of cylindrical surface features in image sequences, enabling the recovery of fine structures; however, this approach relies on richly textured surfaces (Berveglieri and Tommaselli, 2018). To enhance robustness, point clouds have been modeled as Gaussian mixtures for parameter estimation via expectation-maximization (B. Paláncz and Fukuda, 2016). A region-growing algorithm constrained by point normals and surface distances has been proposed, integrating RANSAC denoising for improved reconstruction quality (Yan et al., 2010). Principal component analysis (PCA) combined with robust regression has been employed for noise-tolerant fitting, yet it struggles with thin cylindrical structures (Nurunnabi et al., 2017). Machine learning approaches have been explored for reconstructing narrow cylindrical objects, but challenges remain due to occlusions (Inoue et al., 2021). Despite incorporating various denoising and feature extraction strategies, dense point cloud-based methods remain limited by the density and quality of the point clouds. These methods are unable to effectively compensate for the adverse effects of weak surface textures.

In contrast, sparse feature-based approaches reconstruct cylindrical geometry by estimating parameters from feature points or lines, followed by parametric mesh reconstruction. Yirci et al. (2016) developed a semi-automatic framework that eliminates dependency on texture by requiring manual edge delineation. However, this approach suffers from low automation and lacks validated accuracy. Zheng et al. (2011) proposed a geometric adjustment model that leverages elliptical end-cap features for reconstructing industrial components. Nevertheless, its dependence on observable terminal geometries significantly limits its broader applicability. Ma et al. (2015) integrated cylindrical constraints into bundle adjustment, jointly optimizing camera poses, sparse feature coordinates, and cylinder parameters. While effective in some cases, this method requires dozens of reliable feature points per cylinder, making it unstable for weakly textured targets. These methods demand stringent prerequisites and lack generalizability.

In summary, these unresolved challenges highlight the need for robust reconstruction frameworks tailored to weakly-textured cylindrical objects in photogrammetric applications.

3. Methodology

Artificial cylindrical objects in UAV imagery typically exhibit slender geometries and weakly-textured surfaces, making the detection of robust feature points/lines particularly challenging. Consequently, triangulating surface feature coordinates through conventional photogrammetric approaches proves difficult. To overcome the dependency on point features in classical MVS methods, this paper introduces the concept of tangent dihedral angles based on cylindrical edge features for 3D reconstruction of cylindrical objects: The two planes formed by the bilateral edges of a cylindrical object and the camera optical center are respectively tangent to the cylindrical surface. We define the dihedral angle constituted by these planes as the tangent dihedral angle of the cylindrical object, as shown in Figure 2.



Figure 2. A tangent dihedral angle formed by the camera center C and a pair of edges.

The TDA spatially constrains cylindrical objects within its internal subspace. Theoretically, the geometric parameters (position, orientation, radius) of a cylindrical object can be determined using TDAs from two viewpoints. The reliability of cylindrical geometry estimation improves with both increased quantity of corresponding TDAs and expanded angular disparity between observation perspectives. The actual enveloping effect of multi-view TDAs on cylindrical objects is illustrated in Figure 3. Figure 3 shows a top-down view along the cylinder's axis, where the green annulus represents the cylindrical object and translucent lines indicate corresponding TDAs. These dihedral angles exhibit distinct orientations while maintaining tangency to the cylindrical surface.

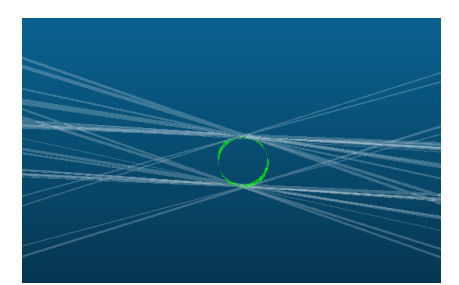


Figure 3. Example of multi-view TDAs enveloping cylindrical object.

Based on this geometric relationship, this paper proposes a 3D reconstruction method for weakly-textured cylindrical objects using TDA constraints derived from edge features in UAV imagery. The method involves first extracting cylindrical edge segments through manual delineation or algorithmic detection and performing local edge pairing. Subsequently, dihedral angles are constructed using paired edges and camera optical centers, followed by establishing correspondence between TDAs. Finally, model parameters including diameter, position, and orientation are solved under multi-view tangency constraints, enabling high-accuracy 3D model reconstruction through mesh generation and texture mapping.

3.1 Edge Pair Generation

The extracted and paired edge line segments form the foundation for subsequent construction and matching of TDAs. To acquire edges of cylindrical objects, either the LSD algorithm (Grompone von Gioi et al., 2012) or learning-based approaches such as SOLD2 (Pautrat et al., 2021) and DeepLSD (R. Pautrat et al., 2023) can be employed for line segment extraction from UAV imagery, with manual delineation supplementing edge features when extraction results prove inadequate. Paired bilateral edges belonging to the same cylindrical object are then identified, serving as inputs for dihedral angle construction with camera optical centers. The edge extraction and pairing performance is demonstrated in Figure 4.



Figure 4. Extracted pairs of edges in a UAV image.

The obtained edge pairs inevitably contain erroneous results that will be filtered out during subsequent processing.

3.2 Correspondence Search

Considering the nearly identical appearance of stay cables, where texture-based matching demonstrates poor reliability, this paper proposes geometric-level matching of edge pairs (tangent dihedral angles). For any tangent dihedral angle <P1, P2> in contact with a cylindrical object, its bisector P3 must necessarily contain the cylinder axis, as demonstrated in Figure 5. The figure illustrates camera optical center C, where two gray triangular planes correspond to P1 and P2 respectively, a green triangular plane represents bisector P3, and a black dashed line indicates the cylinder axis.

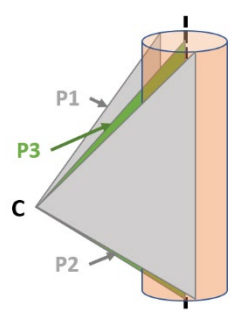


Figure 5. The axis of cylinder lies in the bisector plane.

Consequently, based on the aforementioned geometric properties, the bisectors of corresponding tangent dihedral angles intersect along a spatial line coinciding with the cylinder axis, analogous to how homonymous rays converge at a common spatial point. This principle enables the transformation of TDA matching into bisector matching. The correspondence search task adopts a two-phase strategy: initial seed set generation through three-view matching followed by correspondence expansion to obtain final correspondences.

3.2.1 Seed generation by Three-view matching

The inherent intersection of any two spatial planes precludes geometric determination of plane correspondence through their intersecting relationship due to constraint deficiency. When a third plane introduces redundant information, matching validity can be assessed as follows: Let three planes π_1 , π_2 , π_3 intersect along line L (the cylinder axis). If plane π_3 deviates from the line of intersection between π_1 and π_2 , this geometric inconsistency indicates mismatched planes.

We parameterize the *i*-th TDA bisector as $\pi_i = [a_i, b_i, c_i, d_i]^T$, where the four parameters satisfy:

$$a_i X + b_i Y + c_i Z + d_i = 0 \tag{1}$$

where, (a_i,b_i,c_i) represents the unit normal vector of the plane, and d_i denotes its signed distance to the coordinate origin.

For three bisectors to intersect along a common line, their coefficients must satisfy the following condition:

$$rank(\pi_1, \pi_2, \pi_3) < 3 \tag{2}$$

In other words, there exist real numbers α and β such that equation (3) holds.

"Mobile Mapping for Autonomous Systems and Spatial Intelligence", 20–22 June 2025, Xiamen, China

$$\begin{cases} a_1 = \alpha a_2 + \beta a_3 \\ b_1 = \alpha b_2 + \beta b_3 \\ c_1 = \alpha c_2 + \beta c_3 \\ d_1 = \alpha d_2 + \beta d_3 \end{cases}$$

$$(3)$$

The coefficients α and β are solved using the first three equations of (3), and substituted into the fourth equation to compute the residual $\varepsilon = d_1 - \alpha d_2 + \beta d_3$. A match is confirmed if $\varepsilon < \tau_0$, where the threshold τ_0 is empirically determined based on expected precision. The residual ε shares the same unit as d_i , enabling direct threshold specification.

The seed generation procedure operates as follows:

At first adjacency matrices $N[\cdot,\cdot,\cdot]$ are derived from bundle adjustment results. For images I,J,K, N[I,J,K]=TRUE indicates shared scene overlap. Let S denote the image set. After edge extraction and pairing, each image generates n_I TDAs. The bisector plane of the i-th TDA in image $I \in S$ corresponds to line l_i^I . A cylindrical object's bisector correspondences are represented as $M = (I,i)|I \in S, i \leq n_I, i \in N^*$, with all correspondences stored in $T = \{M_m \mid m = 1, ..., n\}$.

During seed generation, the algorithm iterates over triplets (I,J,K) with N[I,J,K]=TRUE in S. For images I,J,K, all possible bisector triplets $(\pi_i^I,\pi_j^J,\pi_k^K)$ are evaluated. Valid matches satisfying the geometric constraints are recorded as seed correspondences $\{(I,i),(J,j),(K,k)\}$.

3.2.2 Correspondence Expansion

After three-view matching, each seed correspondence M enables computation of the spatial line parameters L_M (direction vector, through point, start/end points) derived from the intersection of three bisectors. Each seed correspondence M in T is then expanded to adjacent images. For M, adjacent images K in set S connected via the adjacency matrix N are identified. The spatial line L_M is projected onto image K as 2D line l_M^K . All projected bisector line segments in K are evaluated: if the distance between l_M^K and the projection of bisector K is below threshold τ_1 , the correspondence (K,k) is added to M, and L_M is recalculated. This iterative process continues until all N-connected images associated with M are processed.



Figure 6. Correspondence expansion steps.

The expansion mechanism is illustrated in Figure 6, which sequentially demonstrates the expansion from three to multiple bisectors. White parallelograms represent image planes; green triangular planes denote validated and expanded bisectors; yellow triangular planes indicate candidate planes formed by intersection lines and target camera centers; red triangular planes signify rejected mismatches; black bold lines depict the consensus cylinder axes of all bisectors.

Upon completion, unexpanded seed (containing only three bisectors) are discarded. Spatial line parameters are recomputed for all remaining matches. Error accumulation may cause deviation between calculated axes $L_{\rm M}$ and true cylinder axes,

resulting in duplicate axis hypotheses. These are merged based on spatial similarity (angular alignment <2°, positional offset <3×GSD) and common observations.

3.3 Cylinder Parameter Estimation via Tangency Constraints

To achieve cylindrical object reconstruction, the geometric parameters (start/end coordinates, central axis parameters, radius) must be determined. Leveraging camera intrinsics/extrinsics and matching results, the cylinder axis is first derived as the intersection line of all bisectors. Subsequently, the axis-aligned start/end points are computed to define the 3D reconstruction scope. As visualized in Figure 7, different parts of a cylindrical object are visible across images, requiring the union of all visibility ranges to accurately determine the complete spatial extent.



Figure 7. A cylindrical object have different visible ranges in multi-view images.

Let r denote the cylinder radius and (X,Y,Z) a point on its axis. The tangency constraint is formulated as:

$$|a_i X + b_i Y + c_i Z + d_i| - r = 0 (4)$$

where a_i, b_i, c_i, d_i are normalized parameters $(a_i^2 + b_i^2 + c_i^2 = 1)$ for computational stability.

Here are four unknown parameters in (4), so the estimation of axis point and radius requires two or more TDAs for stability. The overdetermined systems solved via least squares, enhanced by RANSAC (Fischler and Bolles, 1981; Frahm and Pollefeys, 2006) for outlier rejection. Despite utilizing the adjacency matrix, the two-stage homologous tangent dihedral angle matching process remains inherently exhaustive, exhibiting computational complexity of $O(n^3)$. Therefore, the adoption of partitioning strategies becomes imperative for large-scale datasets to mitigate exponentially increasing computational costs.

3.4 3D Reconstruction

The final 3D reconstruction involves cylindrical surface mesh generation and texture mapping. Standard pipelines (Berra and Peppa, 2020) can be employed for these mature processes.

4. Experiments and Results

The proposed method is implemented in C++ using Visual Studio 2022. For comparative analysis, Bentley Systems' ContextCapture (CC)—a renowned oblique photogrammetry software—is employed as the baseline tool for UAV photogrammetric reconstruction. Notably, the experiments on TDA correspondence search and model parameter estimation utilize CC's sparse reconstruction outputs as foundational data.

The subsequent sections systematically present the experimental dataset, the geometric accuracy evaluation method, and a detailed analysis of the reconstruction results of cylindrical objects.

4.1 Dataset

The Qingshan Bridge is located in Wuhan City, Hubei Province, China. With a total length of 1638 meters, it is supported by 126 pairs of high-strength parallel steel wire cables. The aerial survey was conducted over Qingshan Bridge using a DJI M300 UAV equipped with a P1 full frame camera featuring a 35 mm focal length and a 4.4 µm pixel size. The flight paths strategically planned around a key bridge pier to achieve bidirectional coverage. The dataset comprises 238 images capturing structural components including bridge piers, decks, and cylindrical stay cables. The optimal ground sampling distance (GSD) is 0.2 cm, with an average value of 0.3 cm. Figure 8 illustrates the spatial distribution of image acquisition positions.



Figure 8. Survey overview.

One of the acquired UAV imagery is displayed in Figure 9, demonstrating the fine structure of cables.



Figure 9. Sample UAV image of the Qingshan Bridge.

4.2 Evaluation Method

The positional accuracy of cylindrical objects is inherently ensured by the recovered image poses, making diameter reconstruction accuracy the primary evaluation metric. Quantitative assessment is achieved through comparison between manually measured diameters and the solved values, with the root mean square error (RMSE) serving as the indicator.

4.2.1 Ground Truth Measurement

Field measurements were infeasible due to operational constraints on this vehicular bridge. Leveraging high-accuracy sparse reconstruction outputs, cylindrical diameters were measured by utilizing UAV stereo pairs. As illustrated in Figure 10, representative cylindrical segments were selected for reference measurements.

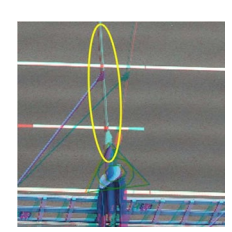


Figure 10. Stereo measurement of cable diameter.

Figure 10 demonstrates diameter measurement in the stereo environment, where demarcated regions indicate cylindrical trunks. Given structural uniformity across test specimens, technicians sampled 8 cylinders, and the ground truth value was derived from repeated measurements along different axial positions. The consolidated reference diameter was established as 16.47 cm through statistical aggregation.

4.2.2 Comparative Methodology

The proposed method was quantitatively compared against CC reconstructions. To evaluate cylindrical diameter accuracy from conventional MVS outputs, geometric parameters were estimated through RANSAC-based cylinder fitting applied to CC-generated dense point clouds. Given inherent noise in photogrammetric point clouds, a modified RANSAC implementation with cylindrical constraints was employed. Target cylindrical point clouds were extracted from CC reconstructions for parameter fitting, with comparative results visualized in Figure 11.

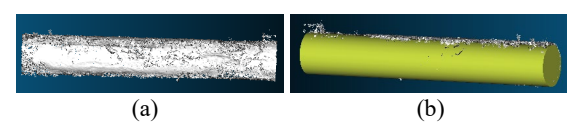


Figure 11. Fitting a cylinder from dense point cloud.

The RANSAC fitting process is demonstrated in Figure 11: (a) shows raw cylindrical point clouds from CC reconstruction, while (b) displays the parametric cylinder generated using fitted geometric parameters. The visual comparison reveals significant surface irregularity suppression through robust fitting.

4.3 Results and Anylasis

4.3.1 Correspondence Validation

The correspondence of tangent dihedral angles across multi-view imagery is visualized through color-coded edge pairs. For validation, two adjacent stay cables (Cable A and B) near the bridge pier were analyzed, with their tangent dihedral angle correspondences marked in cyan and green respectively across different images. As demonstrated in Figure 12, both columns exhibit accurate cross-view correspondence.

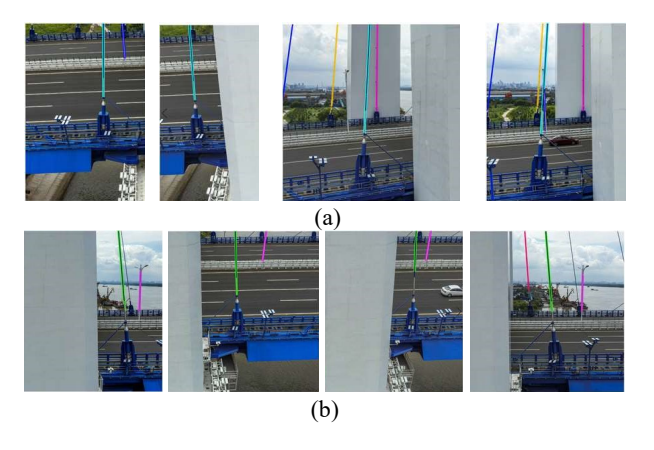


Figure 12. Correspondence visualized for two sample stay cables. (a) Edges of Cable A are colored in cyan; (b) Edges of Cable B are colored in green.

Following successful correspondence search, multi-view tangent dihedral angles spatially envelope the cylindrical object, as shown in Figure 13. This 3D visualization superimposes

reconstructed cylindrical models with their corresponding tangent dihedral angles, represented as semi-transparent triangular planes.

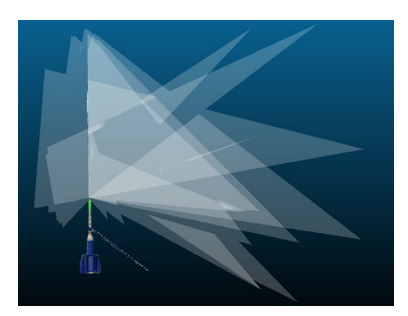


Figure 13. Multi-view corresponding tangent dihedral angles on a stay cable.

The geometric consistency of multiple tangent dihedral angles from diverse viewpoints tangentially constraining a single cylindrical object empirically validates the feasibility of spatial localization through tangent constraints.

4.3.2 Visual Comparison of 3D Reconstruction Results

A comparative analysis of texture-mapped bridge cables and their 3D geometries demonstrates that the proposed method effectively restores the authentic visual characteristics (color and material properties) of real cables. Despite substantial background noise in raw imagery, our approach achieves geometrically and texturally coherent results. A localized comparison of two selected cables between ContextCapture and our method is presented in Figure 14.

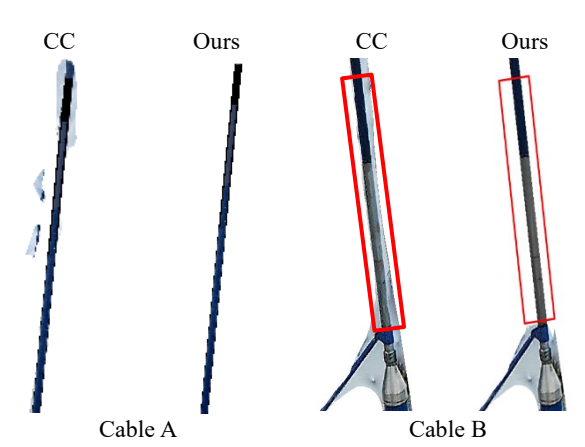


Figure 14. Comparative visualization of cylindrical cable reconstruction result between ContextCapture (CC) and the proposed method

Figure 14 reveals geometric distortions at cylindrical edges in CC reconstructions, whereas our method accurately restores rigid cylindrical structures with continuous curvature and smooth surfaces. Unlike conventional MVS approaches requiring dense stereo coverage, our parametric reconstruction based on geometric parameters (position, diameter, length) succeeds even in regions with partial photographic coverage.

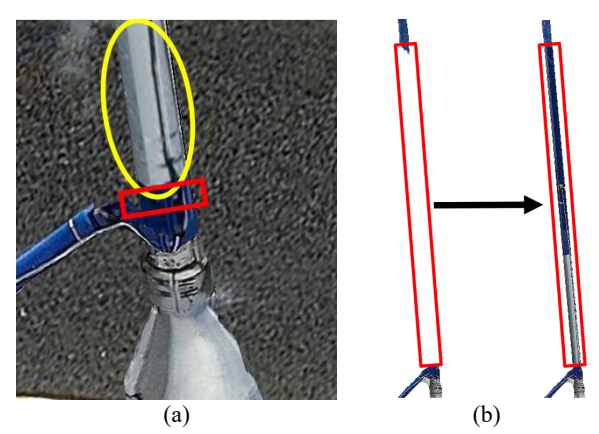


Figure 15. Cylindrical integration in Qingshan Yangtze River Bridge model: (a) Cylindrical cable reconstructed by our method (yellow ellipses) and integration zones (red boxes); (b) Local replacement of CC's model with cable reconstructed by our method.

To evaluate geometric accuracy, cylindrical models generated by our method were integrated into CC-reconstructed scenes (Figure 15). The seamless integration at joints confirms the accuracy of recovered cylindrical positions and radius:

Figure 15(b) demonstrates consistent coloration and texturing across integration boundaries, with no visible misalignment at upper/lower joints. A holistic model comparison (Figure 16) further highlights performance advantages:

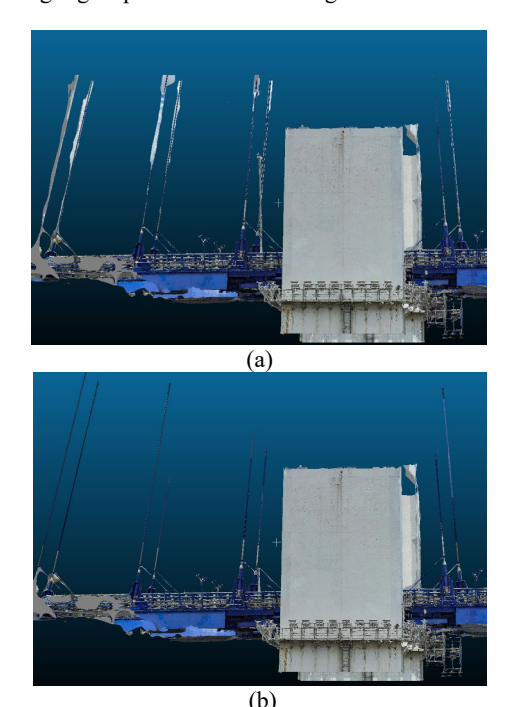


Figure 16. Full-scale reconstruction comparison on bridge piers:
(a) 3D model reconstructed by CC; (b) Replaced the cables generated by our method in CC's model.

CC reconstruction exhibits non-uniform column thickness and twisting deformation, and Our method produces complete, smooth cylinders with enhanced structural fidelity.

The proposed method significantly improves visual quality through geometrically rigorous cylinder parameterization, eliminating artifacts caused by weak textures and occlusions in conventional photogrammetric pipelines.

4.3.3 Reconstruction Accuracy Evaluation

We compared the bridge cable diameters obtained via RANSACbased cylinder fitting from dense matching point clouds with those produced by the proposed method, using the actual diameters as the reference to quantify the reconstruction accuracy.

Manual measurements indicate that the ground truth bridge cable diameter in our dataset is 16.47 cm. The errors in the cylinder diameters estimated by the two methods are summarized as follows:

Cable Index	RANSAC Fitting (CC)		Ours	
	Diameter	Error	Diameter	Error
1	19.12	2.65	16.35	-0.12
2	16.72	0.25	16.38	-0.09
3	14.28	-2.19	16.86	0.39
4	13.91	-2.56	16.52	0.05
5	13.84	-2.63	16.12	-0.35
6	/	/	16.29	-0.18
7	/	/	17.21	0.74
8	/	/	16.48	0.01
	RMSE	2.07	RMSE	0.33

Table 1. Cable diameters & errors by RANSAC Fitting and the proposed method (cm units).

Due to the RANSAC method's reliance on the proportion of inliers in the point cloud, there are cases where the fitting fails. The RMSEs in the final diameter estimates obtained by the two methods are 2.07 cm and 0.33 cm, respectively.

In addition, the diameters estimated by applying RANSAC to MVS 3D reconstruction results exhibit large variance and unstable fitting outcomes. In contrast, the proposed method shows a clear advantage in terms of lower error. Furthermore, since the RANSAC method depends on the inlier ratio, the point clouds of columns 6, 7, and 8 generated by the classical MVS approach were of poor quality, leading to reconstruction failures and inaccurate diameter estimations. Conversely, the proposed method successfully reconstructed all cases, demonstrating superior robustness.

5. Conclusion

In this paper, we propose a UAV photogrammetry-based 3D reconstruction method for cylindrical objects utilizing tangent dihedral angles. The methodology first extracts and pairs linear features from images to obtain bilateral edge pairs of cylindrical objects, constructs tangent dihedral angles using camera optical centers and paired edges, and subsequently establishes TDA correspondences. Cylindrical geometric parameters are then solved under tangency constraints to achieve 3D reconstruction. Comparative experiments with CC reconstructions demonstrate that the proposed method resists interference from cluttered backgrounds and texture-deficient surfaces, significantly improving both geometric positioning accuracy and visual fidelity of cylindrical structures in 3D scenes.

The core innovation lies in its independence from dense point cloud matching, relying solely on cylindrical edge features. This design inherently avoids reconstruction failures caused by weakly-textured surfaces, ensuring superior reliability. Experimental validation on bridge cables confirms robust performance under common imaging conditions. Consequently, the tangent dihedral angle-constrained reconstruction framework

holds significant potential for reconstructing various artificial cylindrical structures in infrastructure inspection, heritage documentation, and industrial surveying applications.

However, the proposed method still presents several limitations. For instance, the accuracy of geometric parameter estimation for cylindrical objects primarily depends on the precision of edge pair extraction, which is influenced by both extraction algorithms and sensor imaging quality. While subpixel-accurate line extraction algorithms (e.g., LSD) are preferable for edge detection, low target-background contrast in complex scenarios leads to high failure rates in automatic extraction, necessitating increased manual intervention costs. Furthermore, processing the dataset containing hundreds of UAV images requires approximately 10 minutes, whereas for ultra-large-scale datasets with over 1,000 images, the computational time during correspondence searching becomes substantial. This highlights the need for algorithmic efficiency improvements in this phase.

Acknowledgements

This study was supported by National Key Research and Development Program of China, No. 2023YFB3905704.

References

B. Paláncz, B.M., J.L. Awange, A. Somogyi, N. Rehány, T. Lovas, Fukuda, Y., 2016. A robust cylindrical fitting to point cloud data. Australian Journal of Earth Sciences 63, 665–673. doi.org/10.1080/08120099.2016.1230147.

Berra, E.F., Peppa, M.V., 2020. Advances and Challenges of UAV SFM MVS Photogrammetry and Remote Sensing: Short Review, in: 2020 IEEE Latin American GRSS & ISPRS Remote Sensing Conference (LAGIRS). 533–538. doi.org/10.1109/LAGIRS48042.2020.9285975.

Berveglieri, A., Tommaselli, A.M.G., 2018. Reconstruction of Cylindrical Surfaces Using Digital Image Correlation. Sensors 18. doi.org/10.3390/s18124183.

Castillo, E., Liang, J., Zhao, H., 2013. Point cloud segmentation via constrained nonlinear least squares surface normal estimates, Chapter 13. Innovations for Shape Analysis: Models and Algorithms, Springer-Verlag, New York.

Chuang, J.-H., Ahuja, N., Lin, C.-C., Tsai, C.-H., Chen, C.-H., 2004. A potential-based generalized cylinder representation. Computers & Graphics 28, 907–918.

Derpanis, K.G., 2010. Overview of the RANSAC Algorithm. Image Rochester NY 4, 2–3.

Fischler, R., Bolles, M., 1981. Random Sample Consensus: A Paradigm for Model Fitting with Applications to Image Analysis and Automated Cartography. Commun ACM 24, 619–638.

Frahm, J.-M., Pollefeys, M., 2006. RANSAC for (Quasi-)Degenerate data (QDEGSAC), in: 2006 IEEE Computer Society Conference on Computer Vision and Pattern Recognition, IEEE, 453–460. doi.org/10.1109/CVPR.2006.235

Furukawa, Y., Curless, B., Seitz, S.M., Szeliski, R., 2010. Towards Internet-scale multi-view stereo, in: 2010 IEEE Computer Society Conference on Computer Vision and Pattern Recognition, IEEE, 1434–1441. doi.org/10.1109/CVPR.2010.5539802.

- Furukawa, Y., Hernández, C., 2015. Multi-View Stereo: A Tutorial. Foundations and Trends® in Computer Graphics and Vision 9, 1–148. doi.org/10.1561/0600000052.
- Grompone von Gioi, R., Jakubowicz, J., Morel, J.-M., Randall, G., 2012. LSD: a Line Segment Detector. Image Processing On Line 2, 35–55.
- Ham, H., Wesley, J., Hendra, H., 2019. Computer Vision Based 3D Reconstruction: A Review. International Journal of Electrical and Computer Engineering 9, 2394–2402.
- Harshit, Jain, K., Mishra, V., 2021. Analysis of survey approach using UAV images and lidar for a Chimney study. Journal of the Indian Society of Remote Sensing 49, 613–618.
- Hu, F., Zhao, J., Huang, Y., Li, H., 2021. Structure-aware 3D reconstruction for cable-stayed bridges: A learning-based method. Computer-Aided Civil and Infrastructure Engineering 36, 89–108.
- Inoue, M., Niigaki, H., Shimizu, T., Honda, N., Oshida, H., Ebine, T., 2021. Visualization of 3D cable between utility poles obtained from laser scanning point clouds: a case study. SN Applied Sciences 3, 860. doi.org/10.1007/s42452-021-04844-6.
- Jiang, S., Jiang, W., Wang, L., 2022. Unmanned Aerial Vehicle-Based Photogrammetric 3D Mapping: A survey of techniques, applications, and challenges. IEEE Geoscience and Remote Sensing Magazine 10, 135–171.
- Kagami, S., Taira, H., Miyashita, N., Torii, A., Okutomi, M., 2020. 3D Pipe Network Reconstruction Based on Structure from Motion with Incremental Conic Shape Detection and Cylindrical Constraint, in: 2020 IEEE 29th International Symposium on Industrial Electronics (ISIE). 1345–1352.
- Kattenborn, T., Sperlich, M., Bataua, K., Koch, B., 2014. Automatic single tree detection in plantations using UAV-based photogrammetric point clouds. The International Archives of the Photogrammetry, Remote Sensing and Spatial Information Sciences 40, 139–144.
- Ladrón de Guevara, I., Muñoz, J., de Cózar, O.D., Blázquez, E.B., 2011. Robust Fitting of Circle Arcs. Journal of Mathematical Imaging and Vision 40, 147–161. doi.org/10.1007/s10851-010-0249-8.
- Langhammer, J., Janský, B., Kocum, J., Minařík, R., 2018. 3-D reconstruction of an abandoned montane reservoir using UAV photogrammetry, aerial LiDAR and field survey. Applied geography 98, 9–21.
- Liang, X., Litkey, P., Hyyppa, J., Kaartinen, H., Vastaranta, M., Holopainen, M., 2012. Automatic Stem Mapping Using Single-Scan Terrestrial Laser Scanning. IEEE Transactions on Geoscience and Remote Sensing 50, 661–670.
- Ma, T., Sun, Z., Zhang, W., Chen, Q., 2015. Three-dimensional reconstruction of a cylinder surface based on constrained bundle adjustment. Optical Engineering 54, 063101.
- Marshall, D., Lukacs, G., Martin, R., 2001. Robust segmentation of primitives from range data in the presence of geometric degeneracy. IEEE Transactions on Pattern Analysis and Machine Intelligence 23, 304–314. doi.org/10.1109/34.910883.

- Miglani, A., Roy, S.D., Chaudhury, S., Srivastava, J.B., 2013. Symmetry based 3D reconstruction of repeated cylinders, in: The Institute of Electrical and Electronics Engineers, Inc.(IEEE) Conference Proceedings. 1–4.
- Nurunnabi, A., Sadahiro, Y., Lindenbergh, R., 2017. ROBUST CYLINDER FITTING IN THREE-DIMENSIONAL POINT CLOUD DATA. The International Archives of the Photogrammetry, Remote Sensing and Spatial Information Sciences XLII-1/W1, 63–70. doi.org/10.5194/isprs-archives-XLII-1-W1-63-2017.
- Pautrat, R., Lin, J.-T., Larsson, V., Oswald, M.R., Pollefeys, M., 2021. SOLD2: Self-Supervised Occlusion-Aware Line Description and Detection, in: Proceedings of the IEEE/CVF Conference on Computer Vision and Pattern Recognition, IEEE, 11368–11378.
- Polat, N., Uysal, M., 2020. An investigation of tree extraction from UAV-based photogrammetric dense point cloud. Arabian Journal of Geosciences 13, 846. doi.org/10.1007/s12517-020-05769-x.
- R. Pautrat, D. Barath, V. Larsson, M. R. Oswald, M. Pollefeys, 2023. DeepLSD: Line Segment Detection and Refinement with Deep Image Gradients, in: 2023 IEEE/CVF Conference on Computer Vision and Pattern Recognition, IEEE, 17327–17336. doi.org/10.1109/CVPR52729.2023.01662.
- Rabbani, T., Van Den Heuvel, F., 2005. Efficient hough transform for automatic detection of cylinders in point clouds. Isprs Wg Iii/3, Iii/4 3, 60–65.
- Rabbani, T., Van Den Heuvel, F., Vosselmann, G., 2006. Segmentation of point clouds using smoothness constraint. International archives of photogrammetry, remote sensing and spatial information sciences 36, 248–253.
- Sarı, B., Hamal, S.N.G., Ulvi, A., 2020. Documentation of complex structure using Unmanned Aerial Vehicle (UAV) photogrammetry method and Terrestrial Laser Scanner (TLS). Türkiye Lidar Dergisi 2, 48–54.
- Yan, L., Xie, H., Zhao, Z., 2010. A new method of cylinder reconstruction based on unorganized point cloud, in: 2010 18th International Conference on Geoinformatics. IEEE, 1–5.
- Zheng, S., Guo, B., Li, C., 2011. 3D Reconstruction and Inspection of Cylinder Based on Geometric Model and Generalized Point Photogrammetry. Acta Geodetica et Cartographica Sinica 40, 477–482.
- Zhu, Y., Xiao, X., Wu, W., Guo, Y., 2023. 3D Reconstruction of deformable linear objects based on cylindrical fitting. Signal, Image and Video Processing 17, 2617–2625. doi.org/10.1007/s11760-022-02478-8.